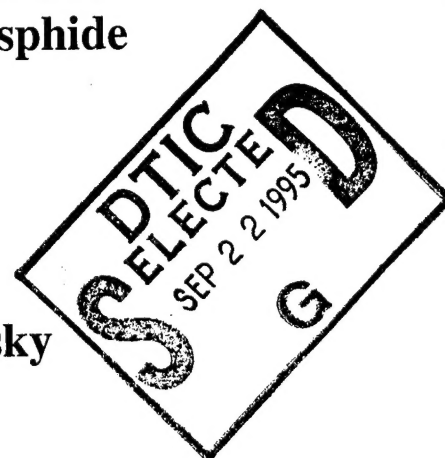FJSRL-TR-95-0006

Electron Paramagnetic Resonance and X-Ray Photoelectron Spectroscopy Investigations of Fe Doped and H^+ Implanted Indium Phosphide

W. Kevin Kuhn
and
Margaret H. Rakowsky

DTIC
SELECTED
SEP 2 2 1995
G

September 1995

AIR FORCE MATERIEL COMMAND

UNITED STATES AIR FORCE

19950919 311

DTIC QUALITY INSPECTED 5

ABSTRACT

In this report, results of electron paramagnetic resonance (EPR), electron nuclear double resonance (ENDOR) and x-ray photoelectron spectroscopy (XPS) studies of iron doped, proton implanted indium phosphide will be presented. The EPR spectra were obtained both as a function of sample angle relative to the magnetic field and as a function of temperature at a given orientation. The results obtained in this study again confirm that the environment around the Fe^{3+} centers is indeed octahedral. In addition, the EPR spectra indicate that there are defects present that behave very much like a spin glass (magnetically diluted defects present in a material with cooperative interactions between the centers that are most distinctly observable at definite temperatures and magnetic field strengths). These results along with the results from the XPS and ENDOR measurements will be presented and discussed in this report.

Accesion For		
NTIS CRA&I		☒
DTIC TAB		☐
Unannounced		☐
Justification		
By		
Distribution /		
Availability Codes		
Dist	Avail and / or Special	
A-1		

Electron Paramagnetic Resonance and X-Ray Photoelectron Spectroscopy Investigations of Fe Doped and H⁺ Implanted Indium Phosphide

INTRODUCTION:

The importance of the III-V semiconductors is clearly evident from the extensive research that has been conducted on these compounds over the past 30 years. [1-10] These studies have identified several compounds that are becoming important for the semiconductor industry. The two most notable of these are gallium arsenide and indium phosphide. Although GaAs devices are currently being used more than InP, InP has several advantages over GaAs. It has a higher thermal conductivity, has enhanced circuit reliability potential due to its superior surface passivation properties, and has better thermal properties which allow for higher current densities.[8] Thus, InP is becoming increasingly important for the manufacture of ultra-high speed devices and substrates for optoelectronic devices.[8,9,11-13] For these applications, however, it is necessary to have a very high quality semi-insulating substrate, and InP grown by the liquid-encapsulated Czochralski method is n-type conductive. Thus, the material is usually doped with iron ($\sim 10^{16}$ cm^{-3}) to obtain the required semi-insulating behavior.[12-22] The iron is most likely a substitutional defect, occupying an indium site[15,19,20,27].

A potential problem influencing the performance of InP devices is the propensity of all III-V semiconductor materials to have hydrogen incorporated into the lattice during growth and processing. Since hydrogen is strongly attracted to dangling bonds, it will readily passivate defects, dopants and impurities present in the material. Thus, if the hydrogen were to migrate during operation, it would alter the characteristics of the device. Therefore, hydrogen passivation needs to be well understood before optimum material performance can be achieved. Ion

implantation is an effective and controllable means of intentionally introducing hydrogen into the semiconductor sample allowing its effects on material properties to be studied.

In this report, results of electron paramagnetic resonance (EPR), electron nuclear double resonance (ENDOR) and x-ray photoelectron spectroscopy (XPS) studies of iron doped, proton implanted indium phosphide will be presented. The EPR spectra were obtained both as a function of sample angle relative to the magnetic field and as a function of temperature at a given orientation. The results obtained in this study suggest that there are defects present in the sample studied that behave very much like a spin glass, where there are magnetically diluted defects with cooperative interactions between the centers that are most distinctly observable at definite temperatures and magnetic field strengths.[23-25] These results along with the results from the XPS and ENDOR measurements will be presented and discussed in this report.

EXPERIMENTAL:

The EPR and ENDOR measurements were conducted with a Bruker ESP 300 X-Band spectrometer operating at 9.458 GHz. A 100 kHz static field modulation was used for EPR spectral acquisition while a 12.5 kHz frequency modulation of the rf field with a 100 kHz modulation depth was used for the ENDOR measurements. The rf input field power was generated using a ENI model A-300 power amplifier. The microwave power was 0.05 mW for both the EPR and ENDOR experiments. Microwave frequencies were measured with a Hewlett Packard 5350B counter. Cryogenic spectral acquisition in the 4-300 K temperature range was accomplished using an Oxford Instruments ESR-900 liquid helium cryostat and the sample temperature was calibrated using the carbon glass sensor supplied with the cryostat. Unless specified otherwise, EPR spectra were acquired at 4 K.

The x-ray photoelectron spectroscopy (XPS) experiments were performed in a Perkin-Elmer Physical Electronics 5600ci ESCA instrument that was equipped with a Mg/Al dual anode x-ray source, a 5 kV differentially pumped ion gun, and a hemispherical electron energy analyzer. The system had a base pressure of $\leq 2 \times 10^{-10}$ Torr with a typical operating pressure of 7×10^{-10} Torr during data acquisition.

The XPS spectra were acquired using an Al K_α x-ray source operating at 400 watts. Sputter cleaning of the samples was performed using Ar^+ ions with a kinetic energy of 3.5 keV and a beam current of 2.5 μA. For the sputter cleaning, the ion beam was rastered over a 2 mm x 2 mm area of the sample with a 40° angle of incidence relative to the sample surface normal. The chamber pressure remaining below 2×10^{-7} Torr while sputtering. The analysis area on the sample was 800 μm in diameter and photoelectron detection was 45° off the surface normal. The sample was held in place on the 25 mm dia. sample holder by two Cu/Be clips. The peak binding energies were corrected for charging by shifting the energy scale such that the carbon 1s peak had a binding energy of 284.8 eV. This procedure gives an experimental uncertainty in the measured binding energies of ± 0.1 eV.

Indium phosphide has a binary tetrahedral crystal structure that crystallizes in a face centered cubic lattice with a $F\bar{4}3m$ space group (zinc blend crystal structure with a lattice constant of 5.865Å) as shown in figure 1. The crystal faces and axes are labeled according to how they will be discussed in this report. The <001> axis is also referred to as the c-axis, and the <100> and <010> axes are similarly referred to as the a- and a'-axes, respectively. The indium phosphide sample used in these experiments was obtained from Dr. Dave Fischer of the Wright Laboratory Materials Directorate and came from boule #0747, wafer #3338, sample #4223. It was iron doped and proton implanted (1×10^{17} cm^{-3} at 2 MeV). The wafer was cut from an

oriented single crystal boule such that the <001> crystal axis was normal to the wafer surface.

X-Ray crystallography indicated that the edges of the square wafer were [110] type planes, thus,

the <100> and <010> axes were oriented along the diagonals of the wafer.

RESULTS AND DISCUSSION:

An EPR spectrum for the iron doped proton implanted InP sample acquired at 4 K with

the <100> axis aligned perpendicular to the EPR magnetic field and the <001> axis parallel to

the field is shown in figure 2. This spectrum is very similar in appearance to the EPR spectrum

of a $3d^5$ ion in an octahedral field (see figure 3). In figure 2, however, the 8:5:9:5:8 fine structure

pattern that is associated with a $3d^5$ electronic configuration (^6S ground state)[12,13,26] is obscured due

to overlap of the outer lines. This overlap is due to the fact that the peaks in this figure are rather

broad, with widths of approximately 200 G. The spectrum shown in figure 2 is, nevertheless,

characteristic for iron doped InP and has been obtained previously by numerous

researchers[12,13,16,17,27] with complete agreement that it arises from Fe^{3+} ions within the indium

phosphide lattice. The spectrum can be analyzed with the usual spin Hamiltonian for an S = 5/2

center in cubic symmetry

$$H = g\beta \mathbf{H} \bullet \mathbf{S} + \frac{a}{6}\left(S_x^4 + S_y^4 + S_z^4 - \frac{707}{16}\right)$$

to obtain the appropriate ESR parameters. This analysis yields a g-factor of 2.023 $\pm$ 0.002 and a

fine structure constant of (220 $\pm$ 5) x 10^{-4} cm^{-1}, respectively. These values are in excellent

agreement with previous studies.[12,13,17,27] The g-factor obtained shows a significant positive shift

from the free electron value of 2.0023. Positive g shifts are associated with electron transfer onto

the central ion from the surrounding ligands, indicating the Fe^{3+} is acting as an electron acceptor.

Figure 4 shows the angular dependence of the EPR spectra arising from these Fe^{3+} centers as the sample is rotated about its <100> axis. In this figure, $0°$ degrees corresponds to the <001> axis being parallel to the magnetic field H. These angle dependent spectra allow one to examine the symmetry of the paramagnetic center being observed. If the environment around the Fe^{3+} center were octahedral, the spectrum at $90°$ would be identical to the spectra at $0°$ and $180°$. In figure 5, the positions of the features observed in figure 4 are plotted as a function of angle to more clearly show the symmetry of the spin. These plots show clearly that there is indeed the 4-fold symmetry that is expected for rotation about a principle axis of a $3d_5$ ion in an octahedral environment. Thus, these figures clearly show that the Fe^{3+} center in the sample analyzed is in a true octahedral environment.

The angular dependence of the spectra acquired upon rotation of the sample about the <001> axis are shown in figure 6. These spectra are ostensibly the same as the spectra shown in figure 4, only with poorer S/N. This a direct result of the physical limitation of the sample tube used. To insert a sample such that the <001> axis would be the axis of rotation, the sample had to be much smaller. Thus, the mass of the sample used for the spectra shown in figure 6 was only 25% of that used for the spectra shown in figure 4. Despite the poor S/N in the spectra shown in figure 6, good peak positions were still obtainable and are shown in figure 7. The plots shown in figure 7 are virtually identical to those seen in figure 5. This further confirms the octahedral nature of the defect site by showing its duplicate nature upon rotation about any of the principle axes of orientation.

Figure 8 shows the angular dependence of the EPR spectra arising from the Fe^{3+} centers as the sample is rotated about its <110> axis. $0°$ degrees corresponds to the <001> axis being parallel to the magnetic field (i.e. same conditions used for the spectrum shown in figure 2). The

spectrum acquired at 0° is identical to the spectrum acquired at 0° degrees in figure 4. This is due

to the fact that even though the axis of rotation is different for the two sets of spectra (figure 4

versus figure 8), because the sample has not yet been rotated, in both cases the <001> axis is

parallel to the magnetic field yielding equivalent orientations of the crystal giving identical

spectra. In figure 9, the angular dependent plots of the data from figure 8 show that there is only

2-fold symmetry for rotation about the <110> axis. In addition, spectra were acquired for

rotation about the <1$\bar{1}$0> axis, however, since these spectra were identical to those shown in

figure 8, they won't be presented here. The symmetry observed in these spectra is again in

agreement with an octahedral crystal field interacting with the Fe^{3+} ions and is in complete

agreement with previously reported angular dependent plots.[28]

Based on the EPR data presented above indicating that the Fe^{3+} center is in an octahedral

environment, it could be postulated that the Fe^{3+} center is located interstitially in the exact center

of a unit cell with four indium nearest neighbors and six phosphorous next nearest neighbors.

This type of unit cell would be exactly the opposite of the one depicted in figure 1 (switch all In

and P atoms). This would explain the observed symmetry since the Fe^{3+} would be surrounded by

six equidistant phosphorous atoms located at the vertices of an octahedron coincident with the

three principle axes of the crystal. The only problem with this postulation is that the IR spectra

of the Fe^{2+} ions in the crystal exhibit tetrahedral crystal field splitting (T_d), implying the Fe ions

are located substitutionally on an indium site.[15,19,20,27] In previous studies,[15,19,20,27,28] it has been

stated that the Fe is only located substitutionally on indium sites in the crystal lattice and that the

Fe^{2+} exhibits tetrahedral crystal field splitting while the Fe^{3+} exhibits cubic (octahedral) crystal

field splitting. Since fairly conclusive arguments can be made[28] that the Fe has to occupy an

indium site (substitutionally), the octahedral symmetry observed in the EPR spectra needs to be

7

reconciled with Fe being located on an indium site in the tetrahedral InP lattice. It is believed[28] that when the iron is doped into the lattice during crystal growth, it gives up three valence electrons to form coordination bonds with the four surrounding phosphorous atoms. This gives the Fe^{3+} centers detected by EPR. Some of these Fe^{3+} atoms will be reduced by the residual donors giving rise to the Fe^{2+} centers observed with IR. As long as more iron is doped into the crystal than is compensated for by the residual donors, the crystal will have the desired semi-insulating properties. The one thing that this doesn't explain, however, is why Fe^{3+} sitting substitutionally on an indium site in the tetrahedral InP lattice exhibits octahedral crystal field splitting in the EPR spectra. It appears that the explanation is that the indium site the iron is occupying, has cubic symmetry due to the overall symmetry of the crystal.[29] Thus the indium would be in an cubic (octahedral) field.

As mentioned earlier, all spectra presented thus far were acquired at 4 K. EPR spectra of transition metal ions are expected to be sensitive to temperature. Due to very fast spin relaxation times, very low temperatures are required to observe the spectra for these paramagnetic centers. For the InP:Fe system being studied here, changing the temperature at which the spectra were acquired, as expected, changes the observed features. The temperature dependence of the Fe^{3+} ion signal with the magnetic field aligned along a principle axis is shown in figure 10. It is clear from this figure that peak intensity decreases as the temperature is increased. Peak position, however, is constant.

Figure 11 shows the temperature dependence of the spectra acquired when the <001> axis is inclined 30° to the magnetic field. In figure 11, the spectra are displayed with a wider magnetic field range (from 1700 G to 5000 G) allowing us to follow the temperature dependence of a broad peak that is present at low magnetic fields. The spectrum acquired at 6 K is

8

essentially identical to the 30° spectrum shown in figure 8, only plotted with a wider magnetic field range. It is clear from this figure that there is indeed an additional paramagnetic center present in the sample, one whose behavior is quite different from that of the Fe^{3+} center presented previously. The reason the data was acquired at 30° with respect to the <001> axis it that at this angle the Fe^{3+} signal is a single peak and therefore won't overlap very much with the newly observed feature allowing a better determination of its peak position. The peak is very broad, with a width of approximately 600 G. The peak position varies with temperature from approximately 2000 to 3000 G.

If the sample is cooled slowly and steadily, this new feature at approximately 2000 G can be enhanced. This is shown in figure 12. The data for this figure were acquired from high to low temperature and clearly show the feature growing in as temperature approaches liquid helium temperatures. In this set of spectra, the low field feature has a width of approximately 300 G. This narrowing of the peak is evidence of the ordering that causes the increase in peak amplitude. In addition, the total peak area increases as the peak grows in. In figure 11, where the peak is broad at low temperatures due to disorder, the integrated peak area is approximately the same as that of the iron peak at 3350 G. In figure 12, however, the integrated area of the low field peak is approximately four times that of the iron peak. The shifts in peak position as a function of temperature are shown in figure 13. From this figure, the g-factor of the low field feature is clearly evident. At low temperatures it is 3.2, but it decreases to 2.2 at higher temperatures. At room temperature the g-factor of this feature is 2.3, and it is the only feature observable.

Figure 14 shows the angular dependence of spectra acquired the same way as for the 6K spectrum in figure 12. Figure 15 is a plot of the peak positions from figure 14. This figure

clearly shows that the spectra arising from the new feature (~2000 G) are rotationally isotropic. This indicates that the center responsible for this feature is not coupled with any other nuclei and that the hyperfine splitting is too small to be measured. The broad width of the peak, however, could easily mask significant hyperfine splitting values.

The behavior exhibited by the feature at low magnetic field are similar to what is observed in spin glass systems.[23-25] In a spin glass, there are magnetically diluted defects with cooperative interactions between the centers that are most distinctly observable at definite temperatures and magnetic field strengths.[23-25] The requirement for specific temperatures and magnetic field strengths is that the signal intensity is dependent on the orientation of individual spins as material is cooled to temperatures cold enough to freeze these spins into an ordered network. Previous work in many different biological systems has observed a broad signal with a g-factor of ~ 3.0.[23] In addition, a study of chloroplast systems[25] found a spin glass type feature with a g-factor of ~ 3.6 at 17 K and ~ 2.3 at 120 K. These vales are not very different from what is shown in figure 13 for the low field peak. A potential problem with the assignment of this peak to a spin glass type feature it the isotropic nature of feature observed in this work. Previous studies have found that the ordered nature of the spins gave a peak that had zero intensity when rotated 90° with respect to the magnetic field.[24] It is believed, however, that there is more evidence in favor of this feature being a spin glass type defect than there is against this conclusion.

Figure 16 shows ENDOR spectra acquired at two different sample orientations. There are clearly angular dependent differences observable, however, a full angle dependent study is needed to fully characterize the angular dependence observed in these two spectra.

Figure 17 is a survey XPS spectrum of the InP:Fe crystal showing that carbon and oxygen are the only major surface impurities. These are most likely due to surface oxides and hydrocarbons as has been observed previously.[11] A survey spectrum acquired after the surface of the crystal was sputter cleaned is shown in figure 18. In this figure only indium and phosphorous are present, indicating that the carbon and oxygen observed in figure 17 are only surface contaminants and are not present in the bulk material. There is no iron signal in the XPS spectra since the iron concentration ($\sim 10^{16}$ cm^{-3}) is well below the XPS detection limit of $\sim 0.1\%$ or $\sim 10^{20}$ cm^{-3}.

Figures 19-21 show high resolution XPS spectra of specific regions of the spectrum presented in figure 18. Figures 19 and 20 show the In $3d_{5/2}$ peak while figure 21 shows the valence band spectra. Phosporous 2p spectra were acquired, but are not presented here since they were essentially the same as what was observed in previous studies.[11] In figure 19, a single peak is present at 444.4 eV for both the proton implanted and non-implanted surfaces. This binding energy is in reasonable agreement with previous data for indium in indium phosphide (444.5 ± 0.2 eV depending on prior surface treatment).[11,30] In figure 20, however, the peak obtained had a binding energy of 444.1 eV. In addition, the peaks presented in figure 20 are broader than those in figure 19. This implies that the observed peaks in figure 20 could be composed of more than one parent peak. By setting a peak at 444.4 eV (indium from InP) and letting a software program fit the observed spectrum, the two peak fits shown in figure 20 were obtained. The peaks added to fit the spectrum are at 444.0 eV. This binding energy definitely corresponds to a reduced form of indium but is not quite the same as metallic indium (443.85 eV).

Figure 21 shows the valence band spectrum for indium phosphide. The spectra obtained in this work are qualitatively similar to previous results.[7] The differences in peak intensities

between the spectra in figures 21a and 21b could be due to the poor signal to noise ratio for these spectra. These spectra show an apparent band gap of ~ 1.0 eV. The term "apparent" is used to describe the band gap since the spectra are broadened due to finite spectral resolution. Thus, a better estimate of the true band gap would probably be that it is closer to 1.5 eV. There appears to be a marked difference between the figure 21a and 21b in the position of the peak at around 10 eV. In the non-implanted surface (and previous work[7]) this peak is observed at 10 - 11 eV. In the implanted surface, however, this peak is clearly located below 10 eV (approximately 9.5 eV). The relation of this peak shift to the proton implantation of the surface is unknown at this time. Further high resolution studies using a monochromatic x-ray source should be conducted to confirm these peak apparent position differences.

CONCLUSIONS:

In this report, the results of EPR, ENDOR, and XPS studies of iron doped, proton implanted indium phosphide have been presented. The EPR spectra were obtained both as a function of sample angle relative to the magnetic field and as a function of temperature at a given orientation. The results obtained in this study again confirm that the environment around the Fe^{3+} centers is indeed octahedral. In addition, the EPR spectra indicate that there are paramagnetic centers present that behave very much like a spin glass. This center is, however, isotropic with respect to rotation about an axis perpendicular to the crossed magnetic and microwave fields. The XPS data show that other than a thin oxide/hydrocarbon layer, the surface is pure indium phosphide. In addition, there is evidence for a reduced form indium near the surface and that this species is more prevalent on the proton implanted surface. The valence band spectra indicate that the band gap is approximately 1.5 eV.

12

REFERENCES

1. *Semiconducting III-V Compounds*, C. Hilsum and A.C. Rose-Innes, eds.; Pergamon Press, New York, NY, 1961.

2. *Optical Properties of III-V Compounds, Vol. 3 in Semiconductors and Semimetals*, R.K. Willardson and A.C. Beer, eds.; Academic Press, New York, NY, 1967.

3. *Physics of III-V Compounds, Vol. 4 in Semiconductors and Semimetals*, R.K. Willardson and A.C. Beer, eds.; Academic Press, New York, NY, 1968.

4. *III-V Compound Semiconductors and Semiconductor Properties of Superionic Materials, Vol 26 in Semiconductors and Semimetals*, R.K. Willardson and A.C. Beer, eds.; Academic Press, Boston, NY, 1988.

5. *Imperfections in III-V Materials, Vol. 38 in Semiconductors and Semimetals*, E.R. Weber, ed.; Academic Press, Boston, NY, 1993.

6. *Minority Carriers in III-V Semiconductors: Physics and Applications, Vol 39 in Semiconductors and Semimetals*, R.K. Altkenkiel and M.S. Lundstrom, eds.; Academic Press, Boston, NY, 1993.

7. L. Ley, R.A. Pollak, F.R. McFeely, S.P. Kowalczyk and D.A. Shirly, *Phys. Rev. B*, **9(2)** (1974) 600.

8. *Indium Phosphide: Crystal Growth and Characterization, Vol 31 in Semiconductors and Semimetals*, R.K. Willardson and A.C. Beer, eds.; Academic Press, Boston, NY, 1990.

9. A.P. Seitsonen, R, Virkkunen, M.J. Puska and R.M. Nieminen, *Phys. Rev. B*, **49(8)** (1994) 5253.

10. T.A. Kennedy and N.D. Wilsey, *Appl. Phys. Lett.,* **44(11)** (1984) 1089.

11. P.A. Bertrand, *J. Vac. Sci. Technol.*, **18(1)** (1981) 28.

12. G.H. Stauss, J.J. Krebs and R.L. Henry, *Phys. Rev. B*, **16(3)** (1977) 974.

13. H.J. von Bardeleben, D. Stievenard, K. Kainosho and O. Oda, *J. Appl. Phys.*, **70(12)** (1991) 7392.

14. P. Dreszer, W.M. Chen, K. Seendripu, J.A. Wolk, W.Walukiewicz, B.W. Liang, C.W. Tu and E.R. Weber, *Phys. Rev. B*, **47(7)** (1993) 4111.

15. H. Ch. Alt, R. Treichler and J. Volkl, *Appl. Phys. Lett.*, **59(27)** (1991) 3651.

16. F.X. Zach, E.D. Bourred, D. Bliss, E.R. Weber and E.E. Haller, Proceedings of the *4th International Conf. on Indium Phosphide and Rel. Materials*, 1992, p638.

17. F. Zach, *J. Appl. Phys.*, **75(12)** (1994) 7894.

18. F.K. Koschnick, M. Rac, J.-M. Spaeth and R.S. Eachus, *J. Phys.: Condens. Matter*, **5** (1993) 733.

19. K. Thonke and K. Pressel, *Phys. Rev. B*, **44(24)** (1991) 13418.

20. K. Pressel, K. Thonke, A. Dornen and D. Pensl, *Phys. Rev. B*, **43(3)** (1991) 2239.

21. H.C. Cookham, T.A. Kennedy and D.J. Treacy, *Phys. Rev.B*, **46(3)** (1992) 1377.

22. D.Y. Jeon, H.P. Gislason, J.F. Donegan and G.D. Watkins, *Phys. Rev. B*, **36(2)** (1987) 1324.

23. A.I. Tsapin, S.V. Khangulov, D.Sh. Burbayev and L.A. Blyumenfel'd, *Biophysics*, **29(6)** (1984) 1073.

24. A.I. Tsapin, O.P. Samoilova, Ye.V. Solodkaya and V.S. Mikoyan, *Biophysics,* **33(4)** (1988) 770.

25. L.A. Blumenfeld, D.Sh. Burbaev, A.I. Tsapin and S.V. Hangulov, *Biofisika*, **23** (1978) 614.

26. J.E. Wertz and J.R. Bolton, *Electron Spin Resonance: Elementary Theory and Practical Applications*, Chapman and Hall, New York, NY, 1986.

27. W.H. Koschel, U. Kaufmann and S.G. Bishop, *Solid State Commun.*, **21** (1977) 1069

28. G.K. Ippolitova, E.M. Omel'yanovskii, N.M. Pavlov, A.Ya. Nashel'skii and S.V. Yakobson, *Sov. Phys. Semicond.*, **11(7)** (1977) 773.

29. T.L. Estle, *Phys. Rev.*, **136(6A)** (1964) A 1702.

30. *Practical Surface Analysis - Volume 1: Auger and X-Ray Photoelectron Spectroscopy*, 2nd Edition, D. Briggs and M.P. Seah, eds., John Wiley & Sons, Chichester, England, 1990.
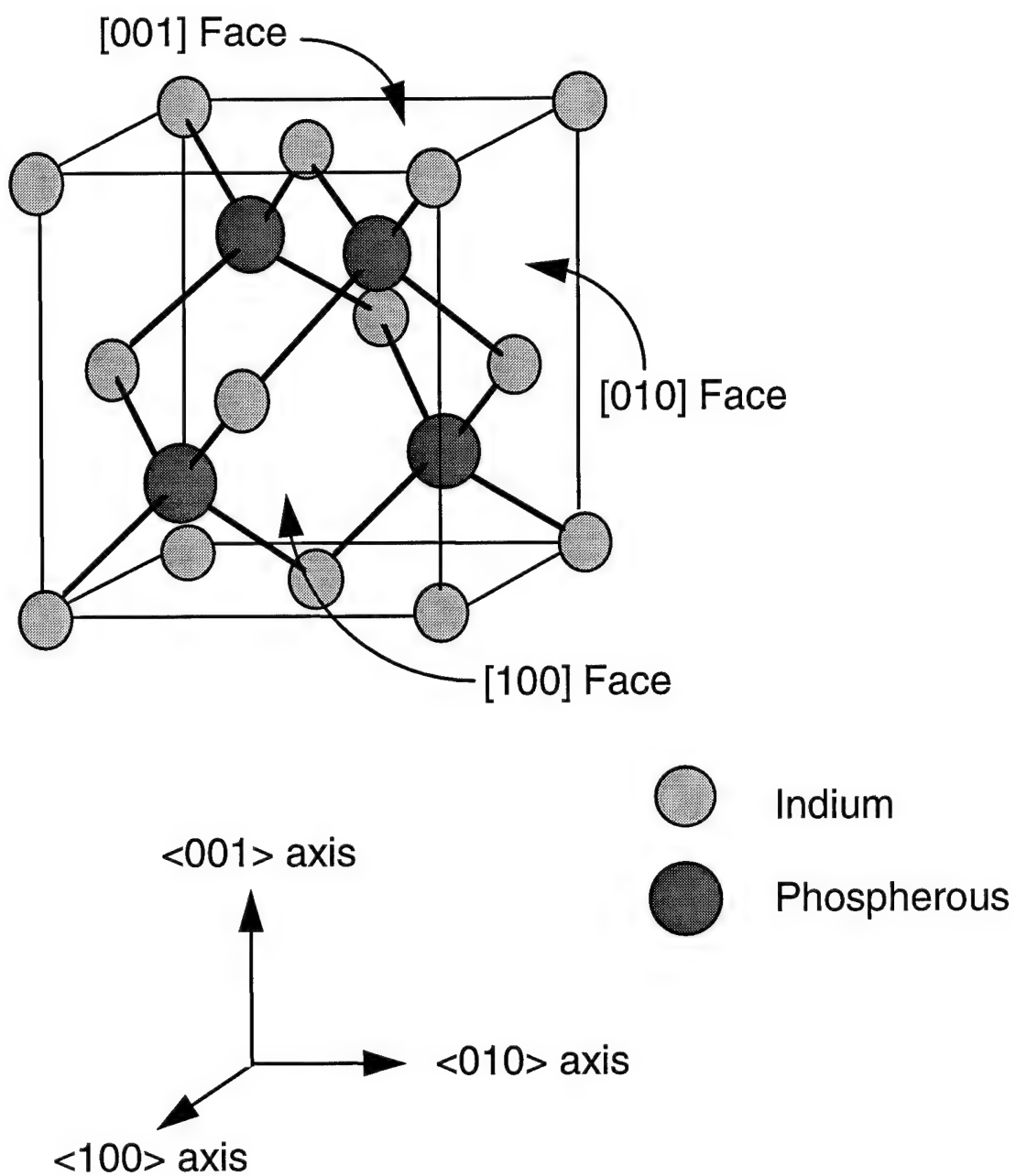
Figure 1: Crystal structure of Indium Phosphide showing orientation of crystal faces and axes.
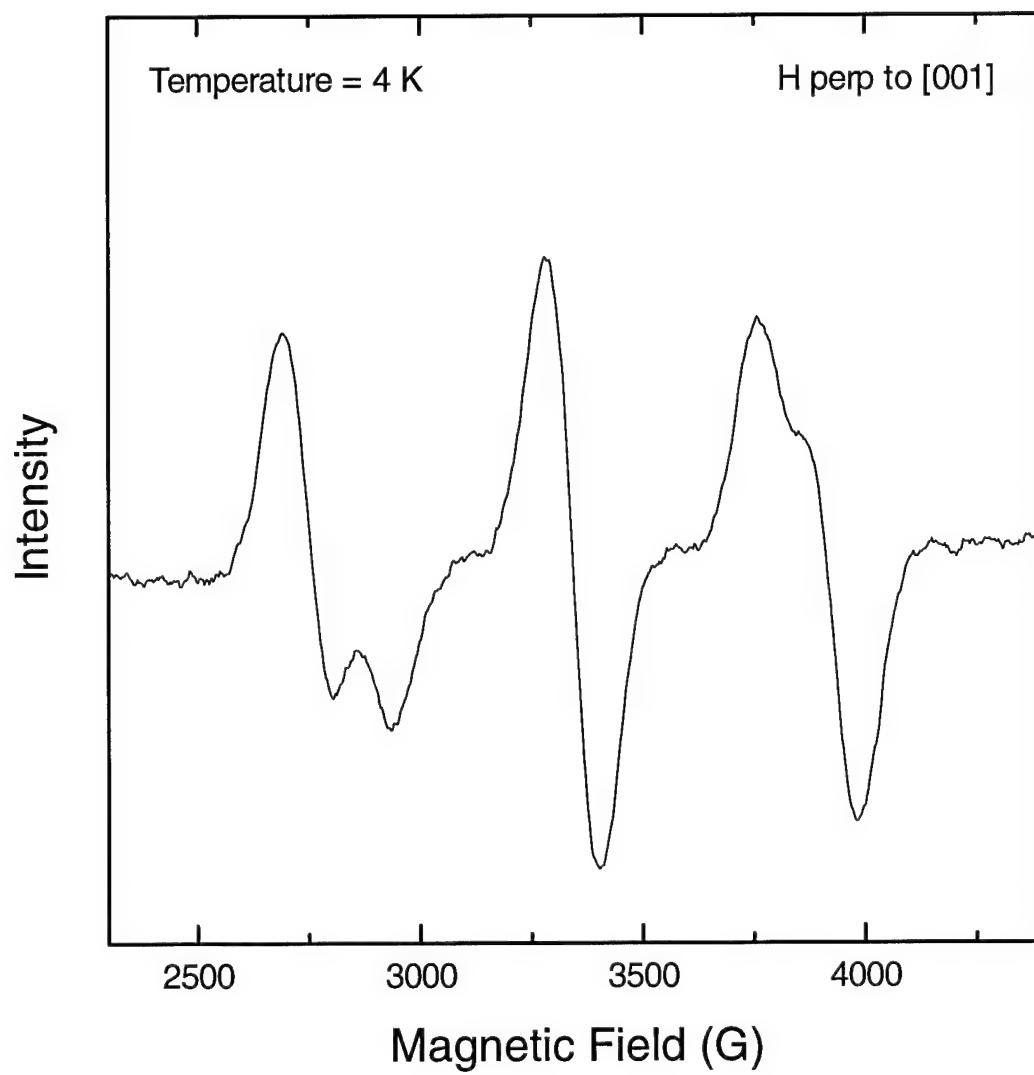
Figure 2: EPR spectrum of Indium Phosphide at 4 K with the magnetic field parallel to the
<001> axis.
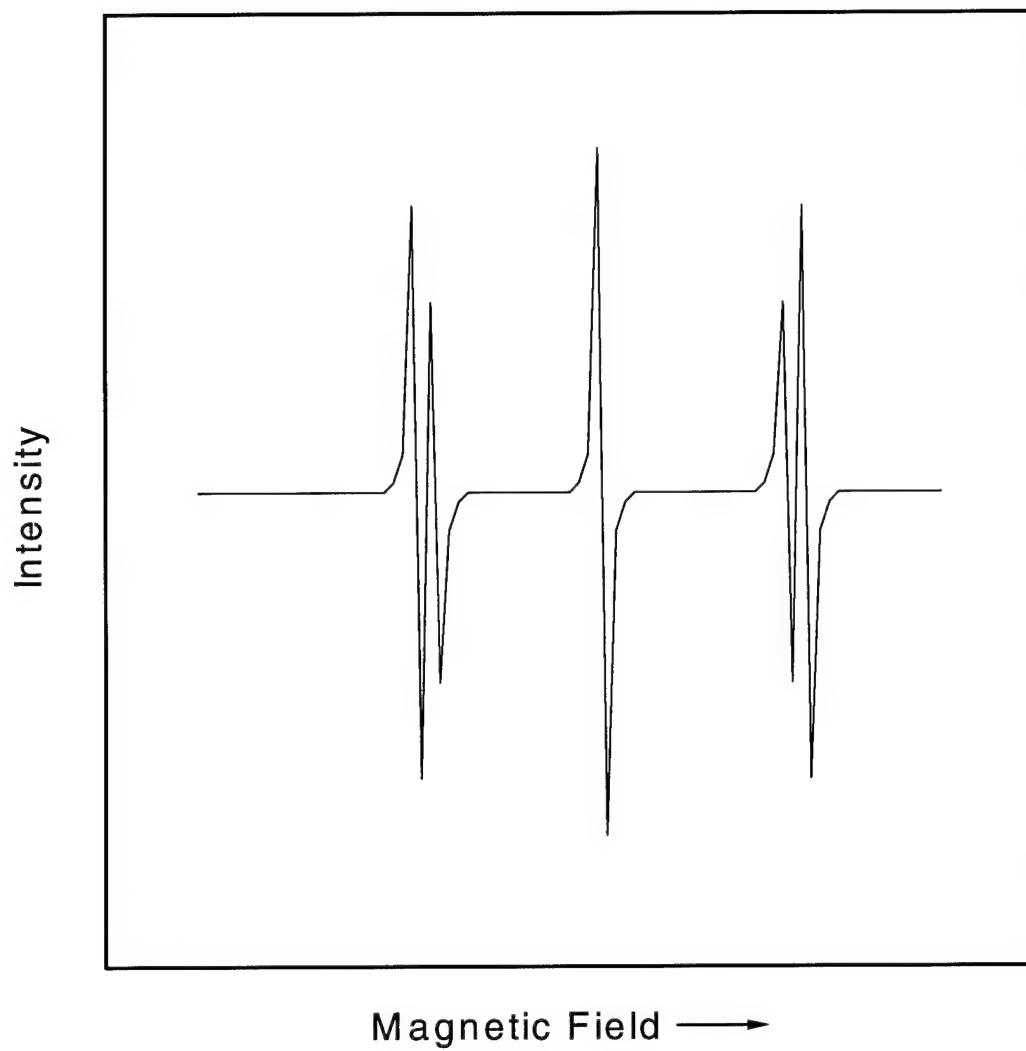
Figure 3: Simulated EPR spectrum of a 3d^5 ion in an octahedral crystal field with the magnetic field (H) parallel to a principal axis of the octahedron.
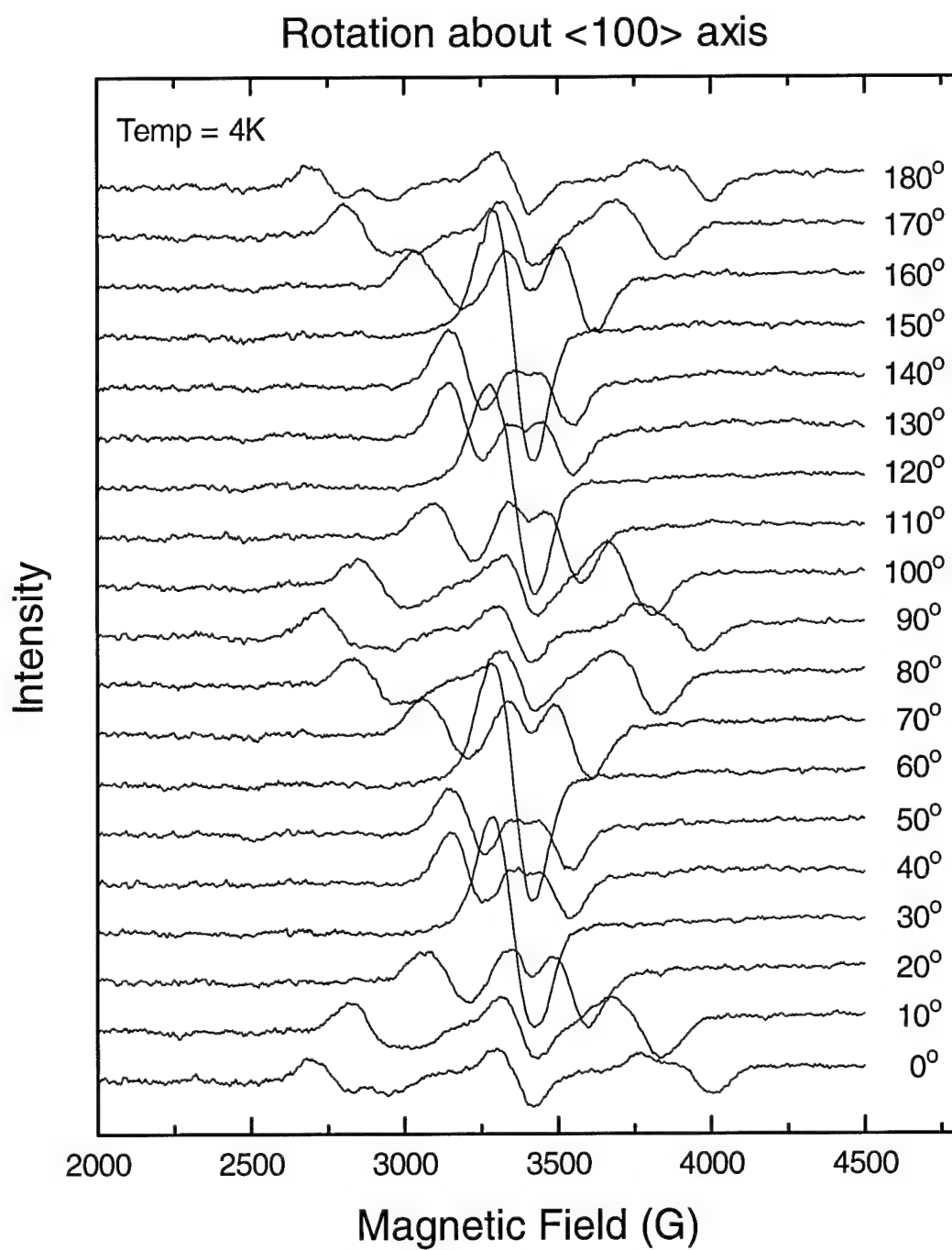
Figure 4: Angular dependence of EPR spectra at 4 K upon rotation about <100> axis. 0°
corresponds to the <001> axis being parallel to the magnetic field H.

a)
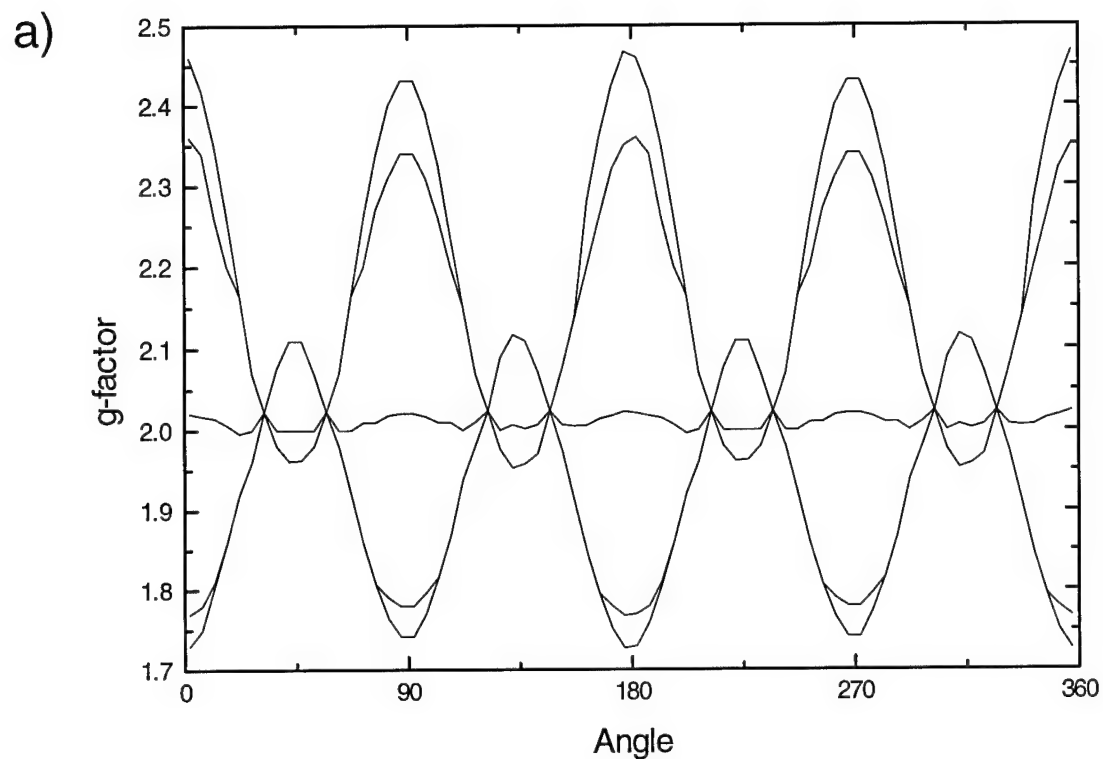
b)
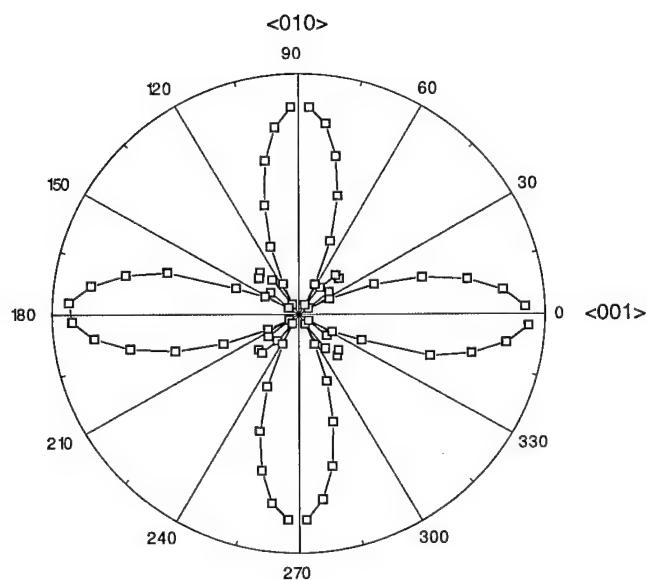
Figure 5: Graphical representation of the angular dependence of the features in the EPR spectra shown in figure 4 showing defect symmetry: a) cartesian coordinates, b) polar coordinates showing the spread between the maximum and minimum g-factor features.

Rotation about <001> axis
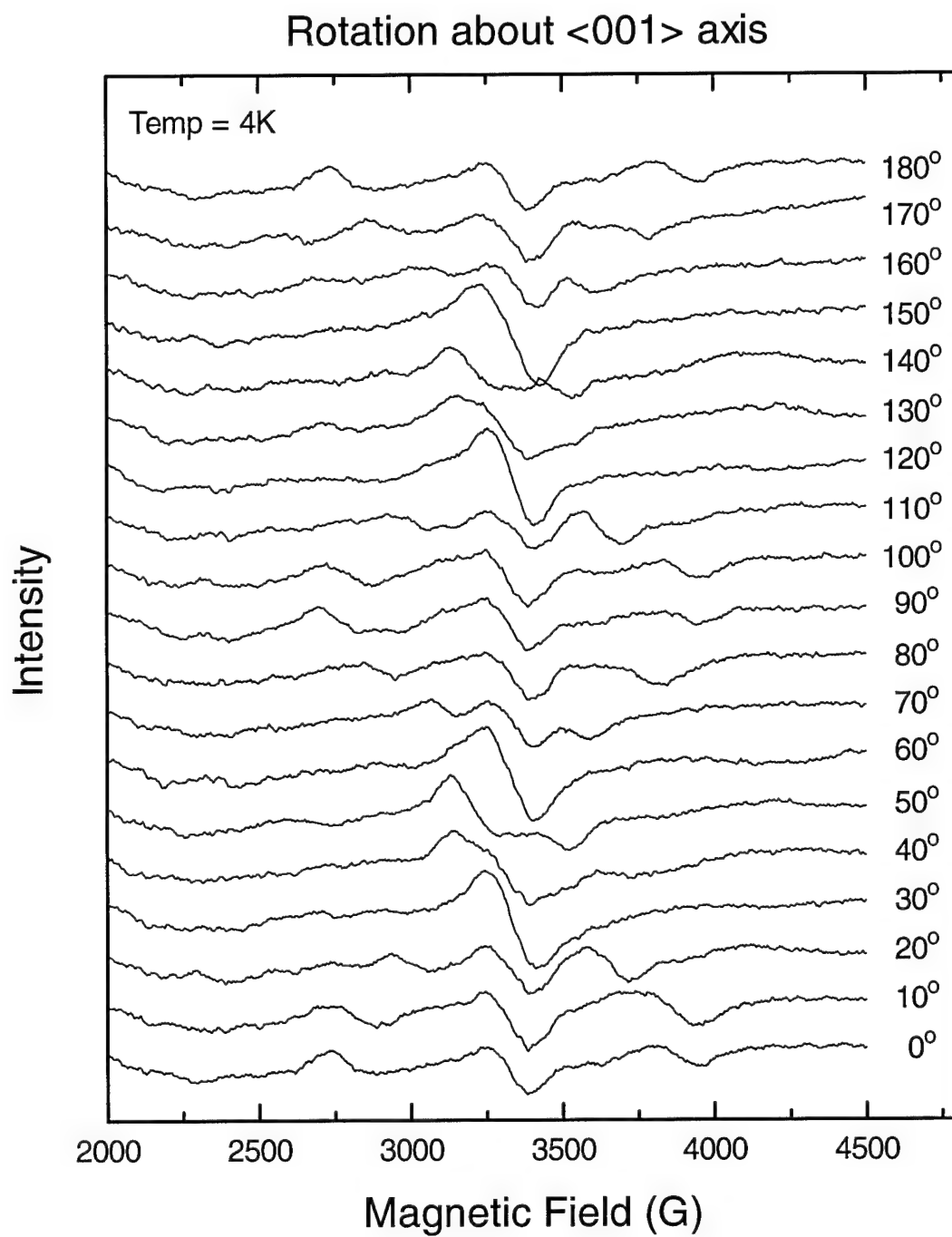
Figure 6: Angular dependence of EPR spectra at 4 K upon rotation about <001> axis. 0°
corresponds to the <100> axis being parallel to the magnetic field H.

a)

b)

<010>

<100>
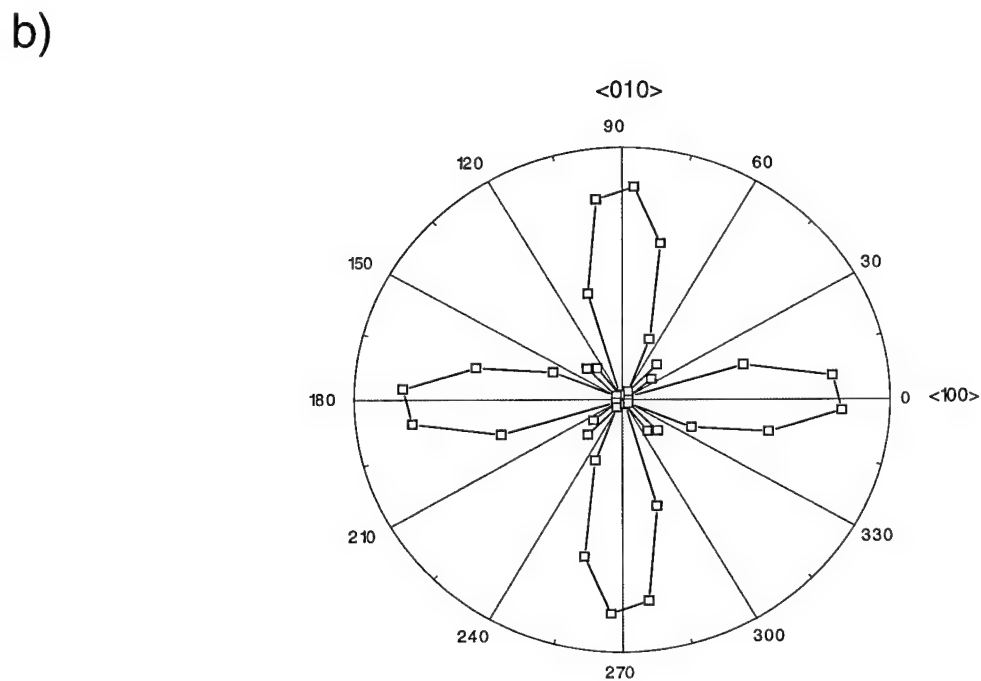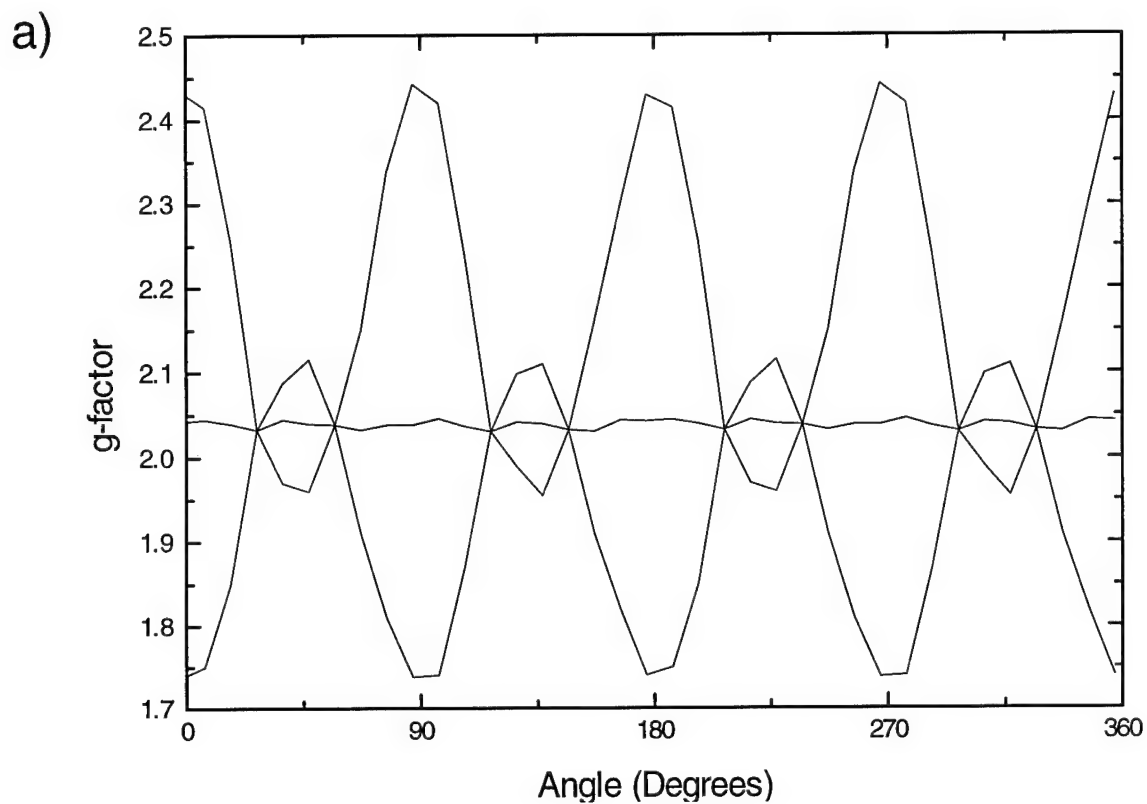
Figure 7: Graphical representation of the angular dependence of the features in the EPR spectra shown in figure 8 showing defect symmetry: a) cartesian coordinates, b) polar coordinates showing the spread between the maximum and minimum g-factor features.

21
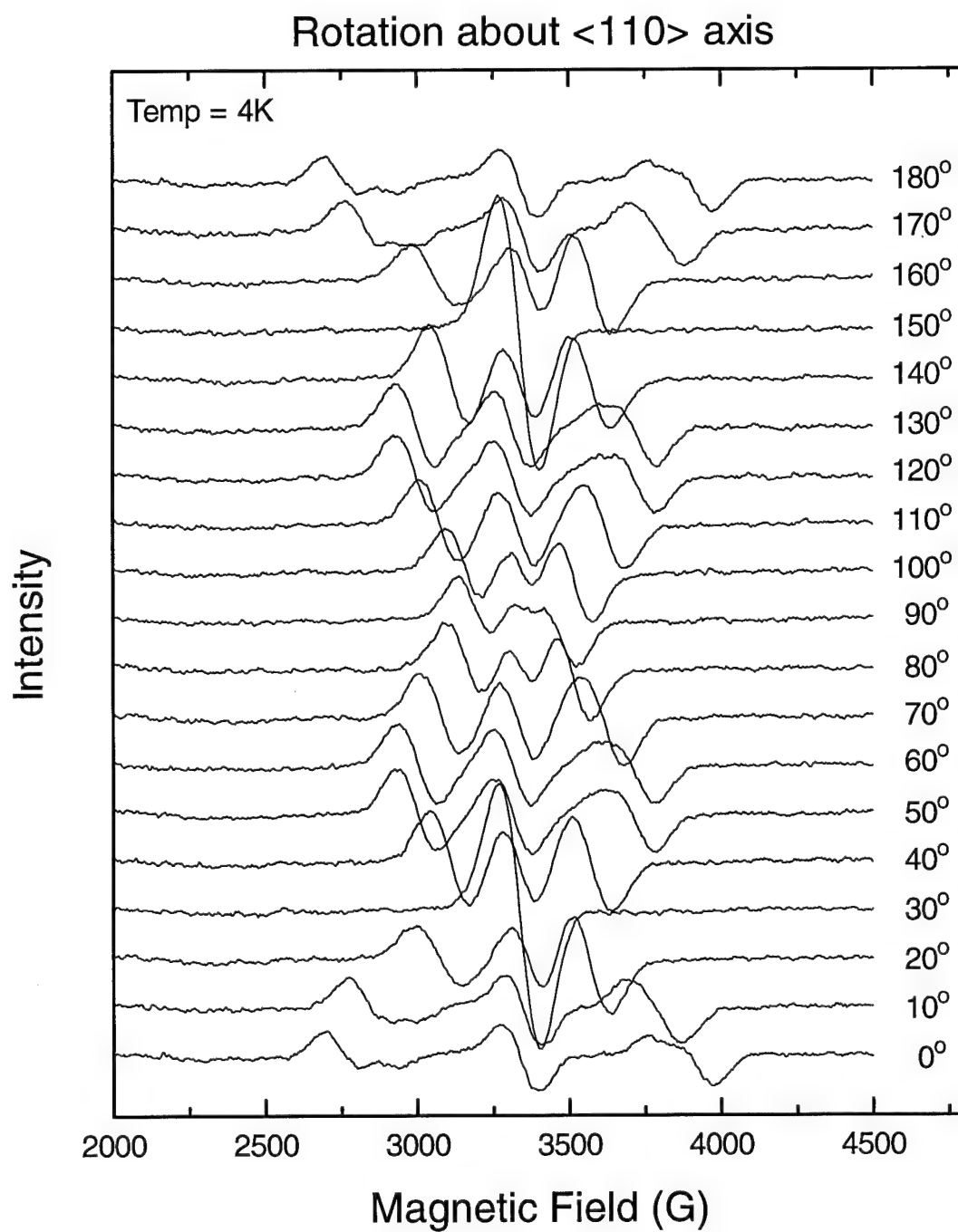
Figure 8: Angular dependence of EPR spectra at 4 K upon rotation about <110> axis. 0° corresponds to the <001> axis being parallel to the magnetic field H.

a)

b)
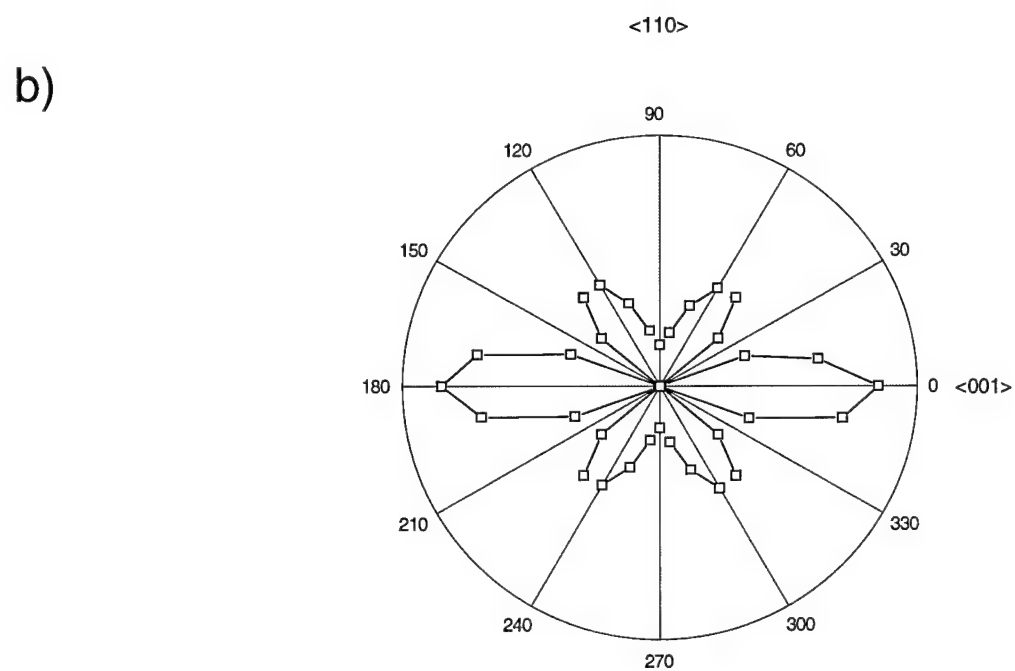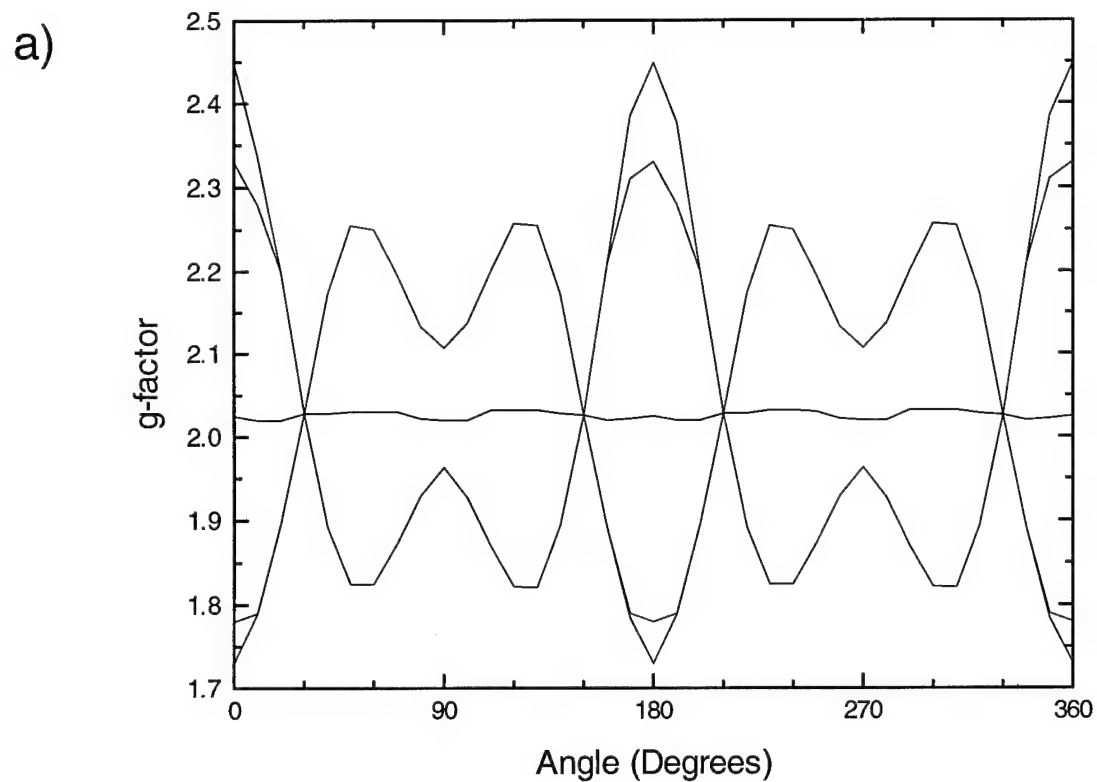
Figure 9: Graphical representation of the angular dependence of the features in the EPR spectra shown in figure 6 showing defect symmetry: a) cartesian coordinates, b) polar coordinates showing the spread between the maximum and minimum g-factor features.

Temperature Dependence
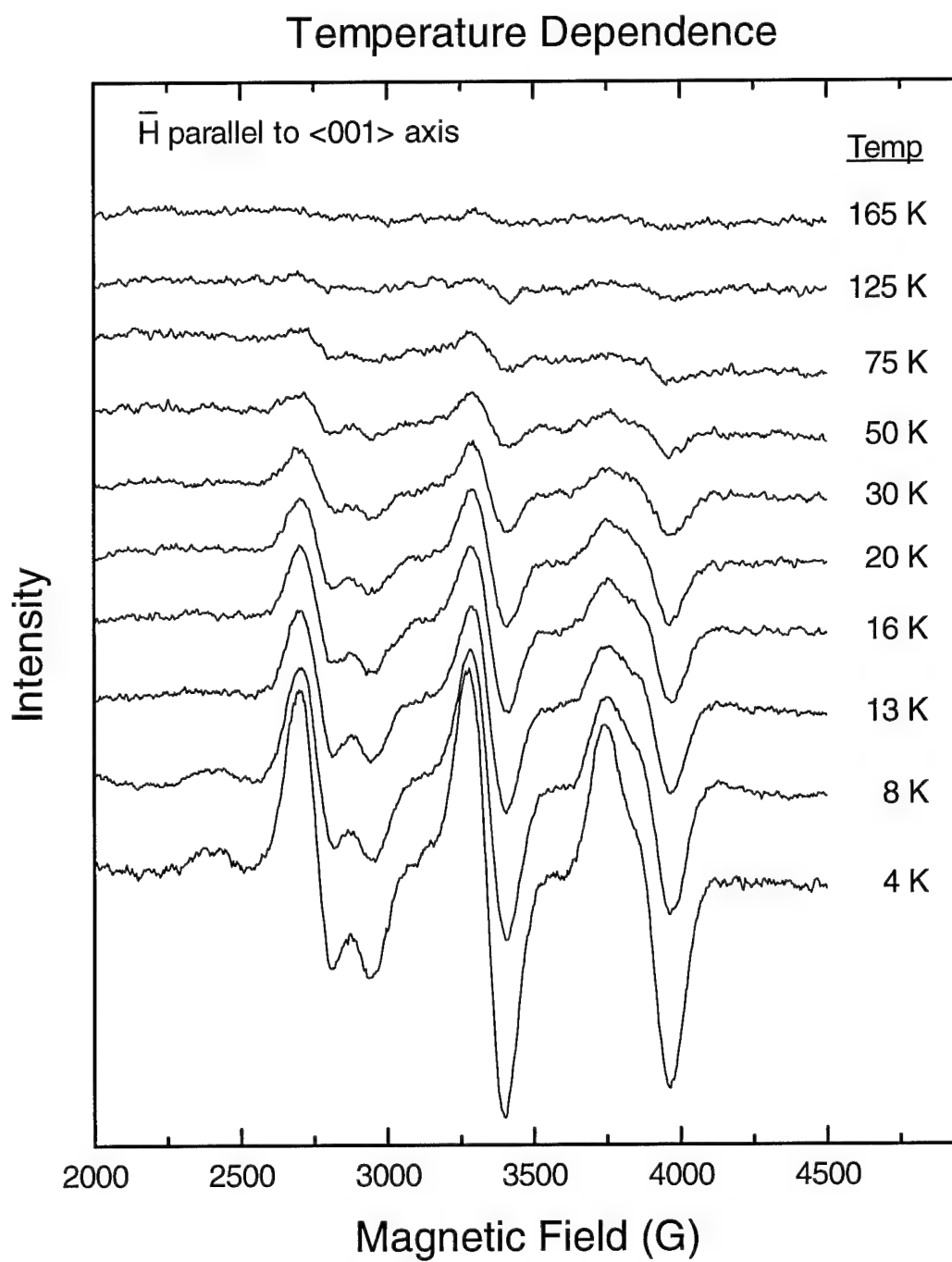
Figure 10: Temperature dependence of the EPR signal with the magnetic field parallel to the <001> axis and perpendicular to the <110> axis.
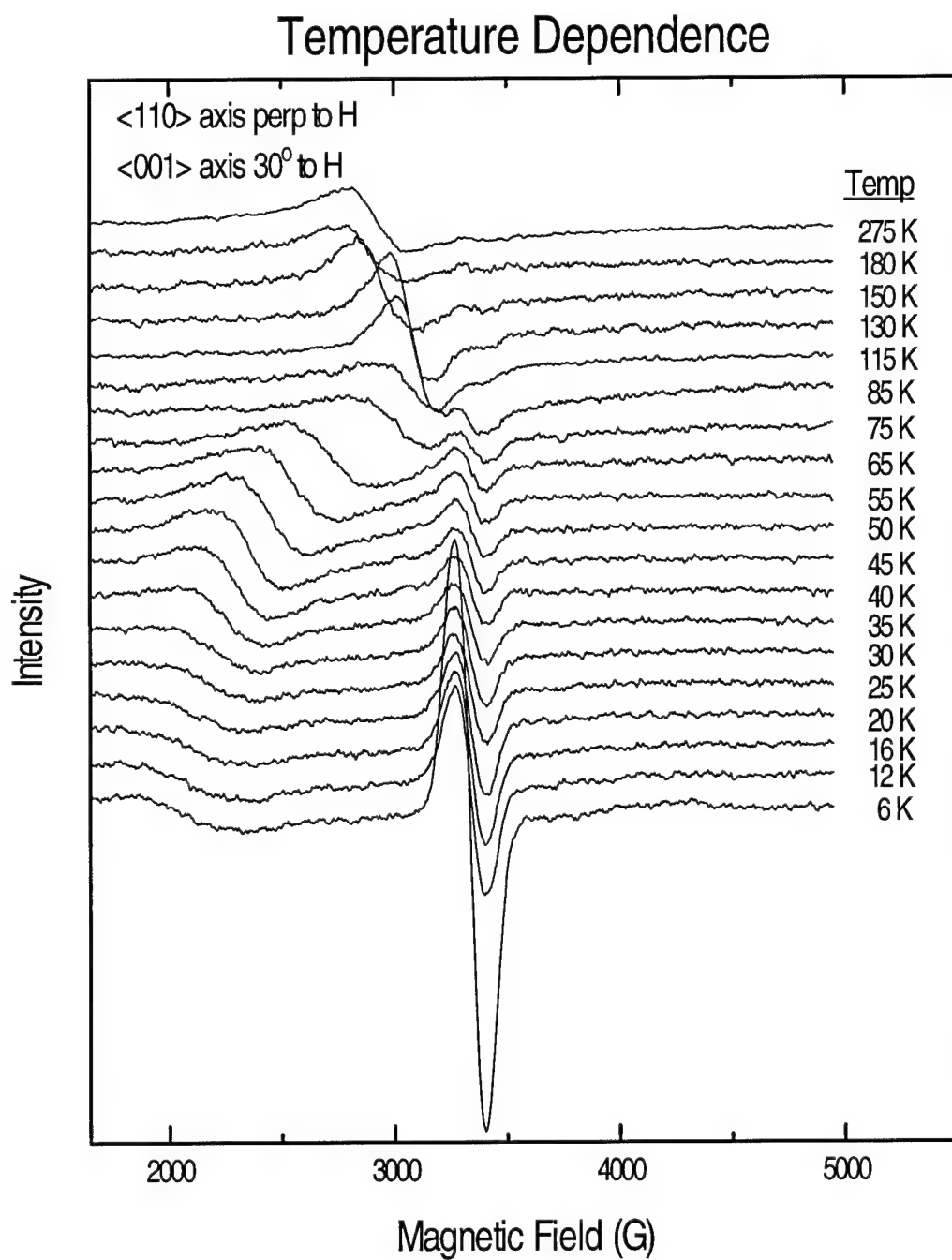
Figure 11: Temperature dependence of the EPR signal with the magnetic field 30° to the <001> axis and perpendicular to the <110> axis.

Temperature Dependence

<110> axis perp to H

<001> axis 30° to H

Temp

180 K
150 K
130 K
115 K
85 K
75 K
63 K
50 K
41 K
30 K
20 K
15 K
10 K
8 K
5 K

Intensity

Magnetic Field (G)

2000   3000   4000   5000
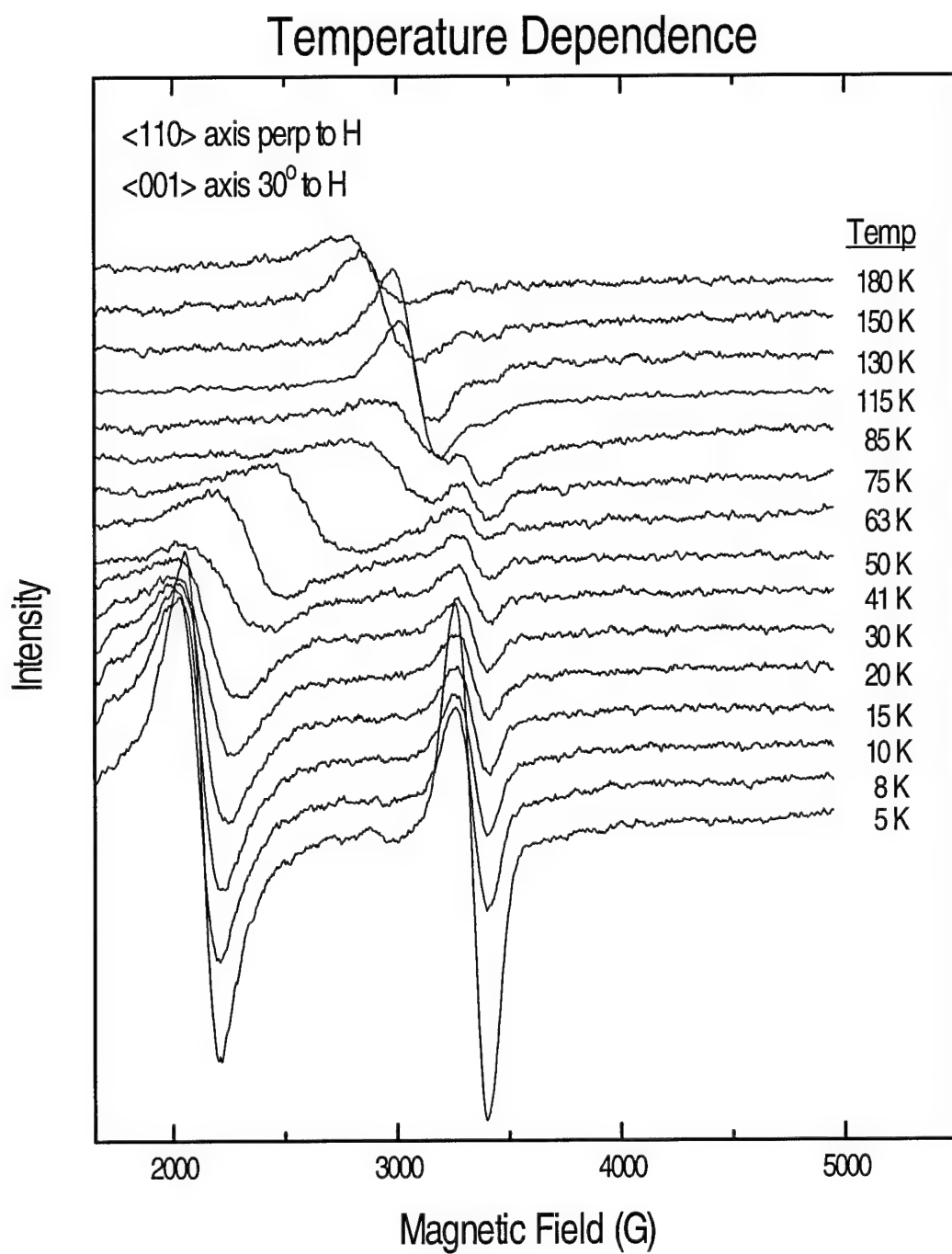
Figure 12: Temperature dependence of the EPR signal with the magnetic field 30° to the <001> axis and perpendicular to the <110> axis. Low field peak prominent at low temperatures due to careful sample cooling.
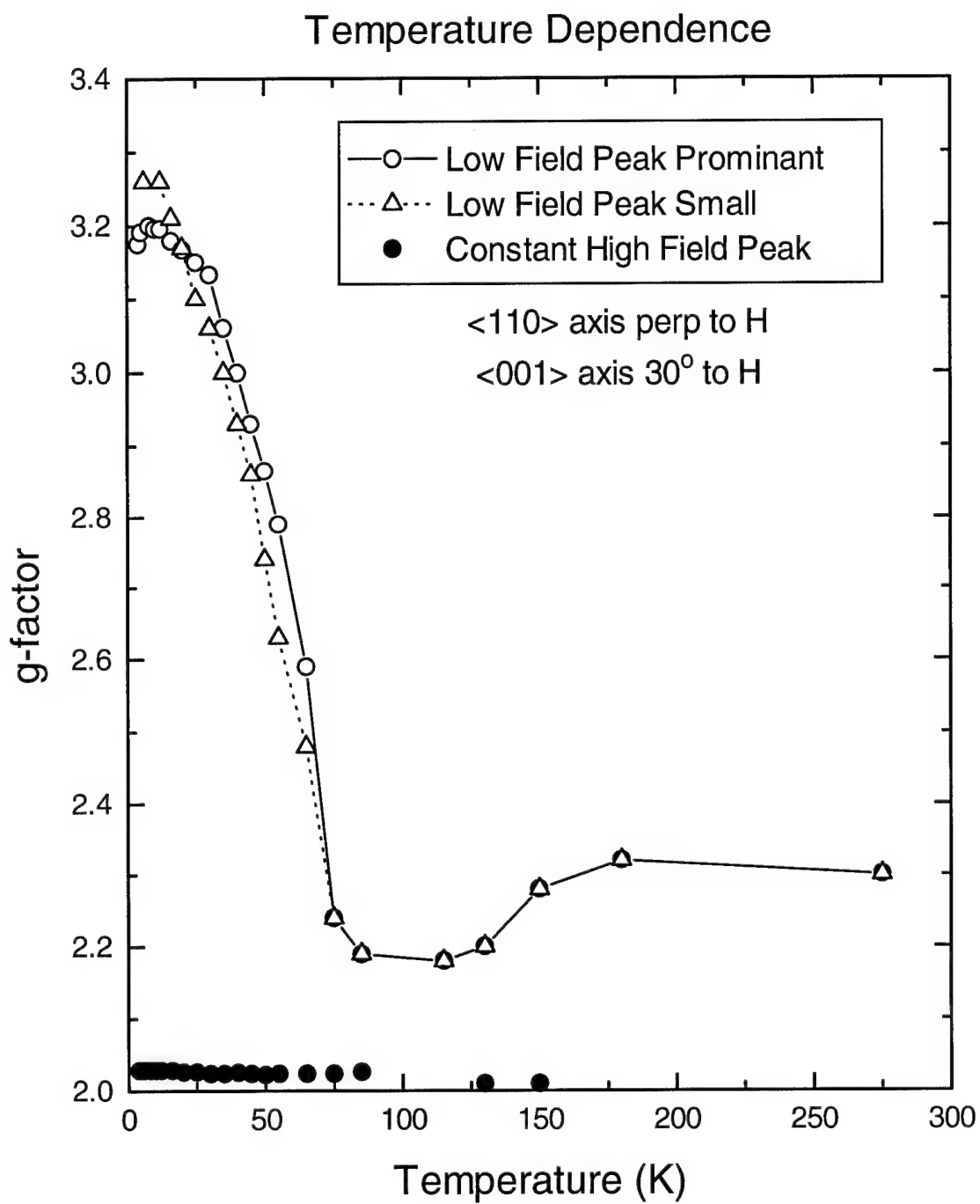
Figure 13: Temperature dependence of the EPR signal with the magnetic field 30° to the <001> axis and perpendicular to the <110> axis.
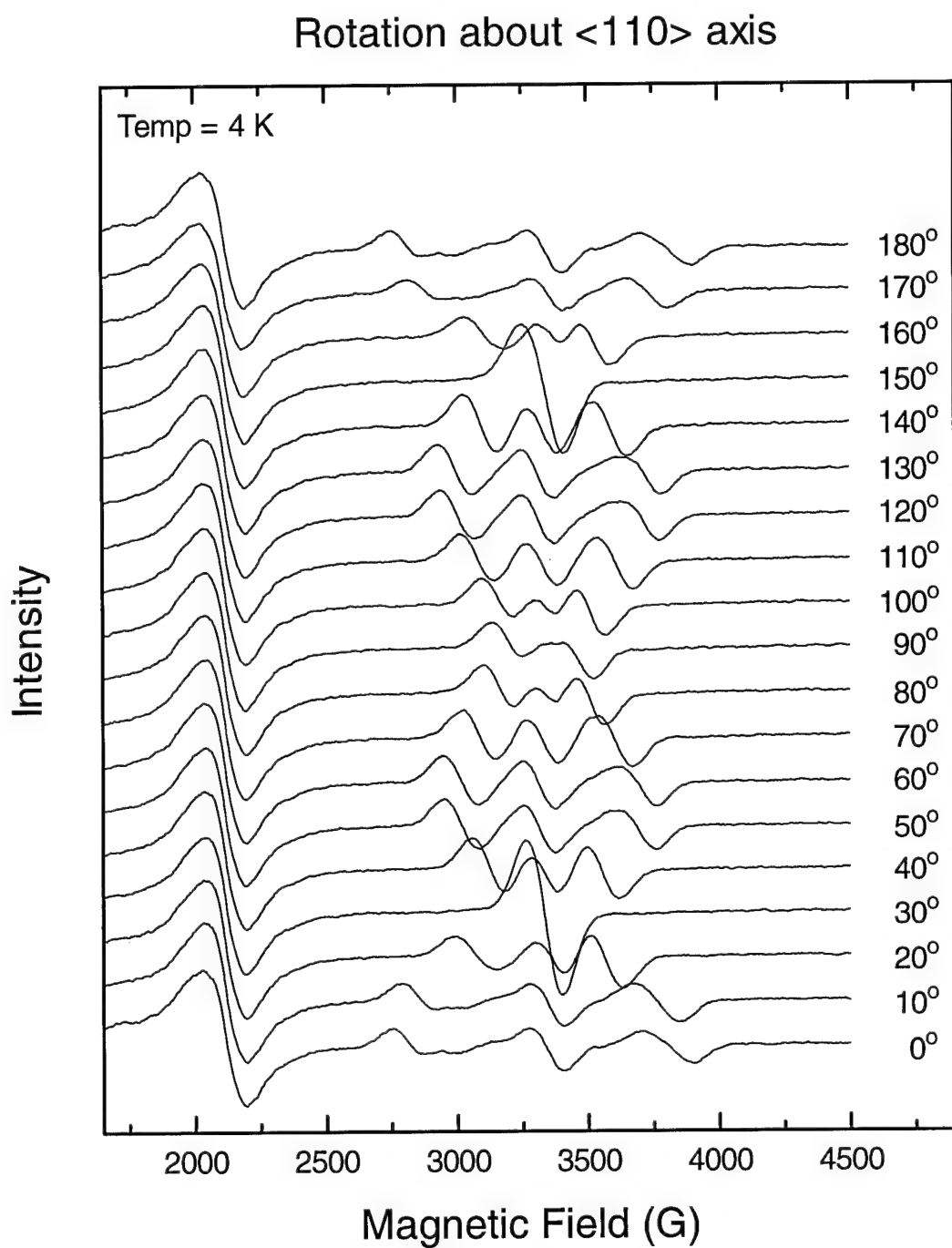
Figure 14: Angular dependence of EPR spectra at 4 K upon rotation about <110> axis. Low field peak is prominent due to careful sample cooling. 0° corresponds to the <001> axis being parallel to the magnetic field H.
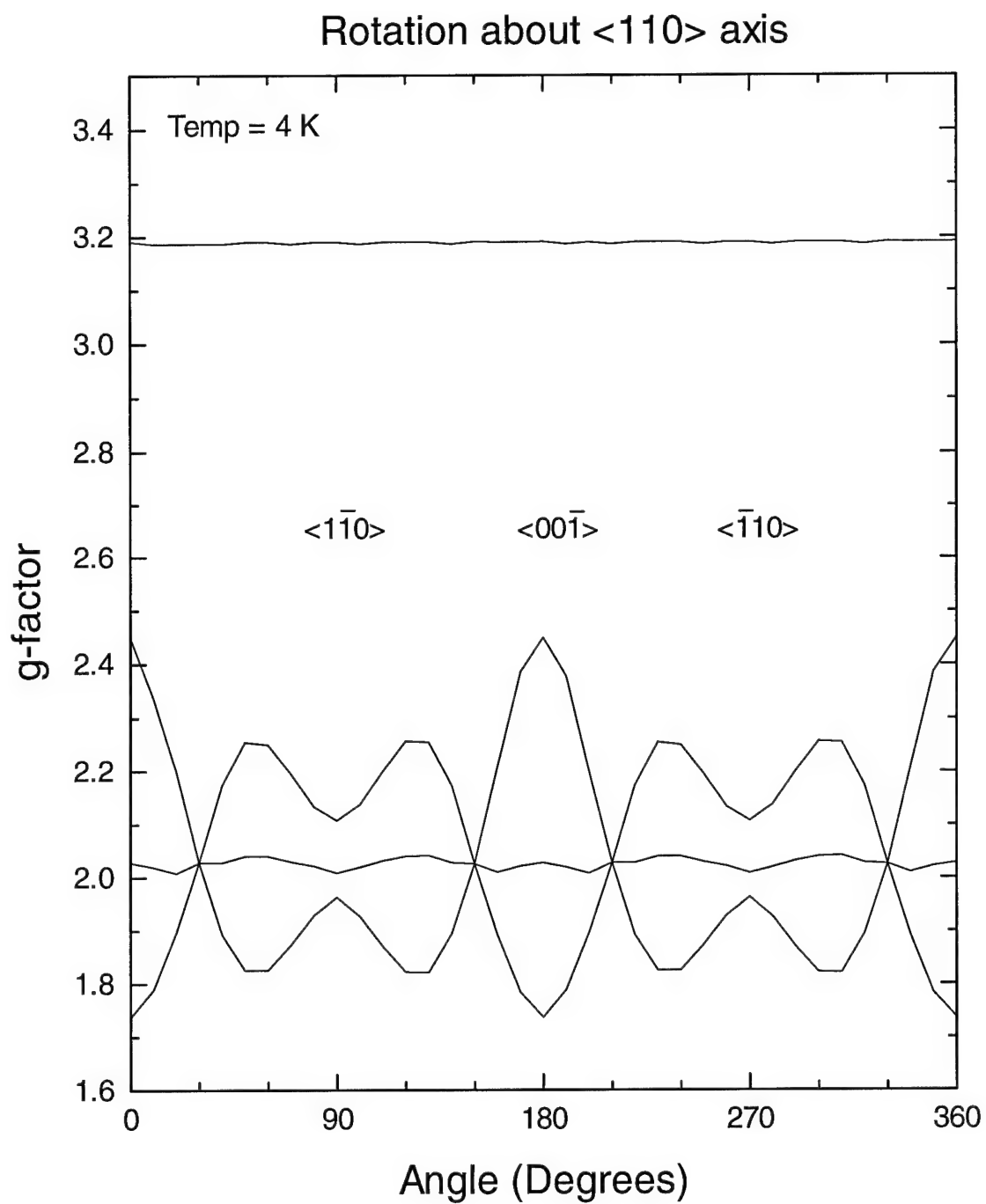
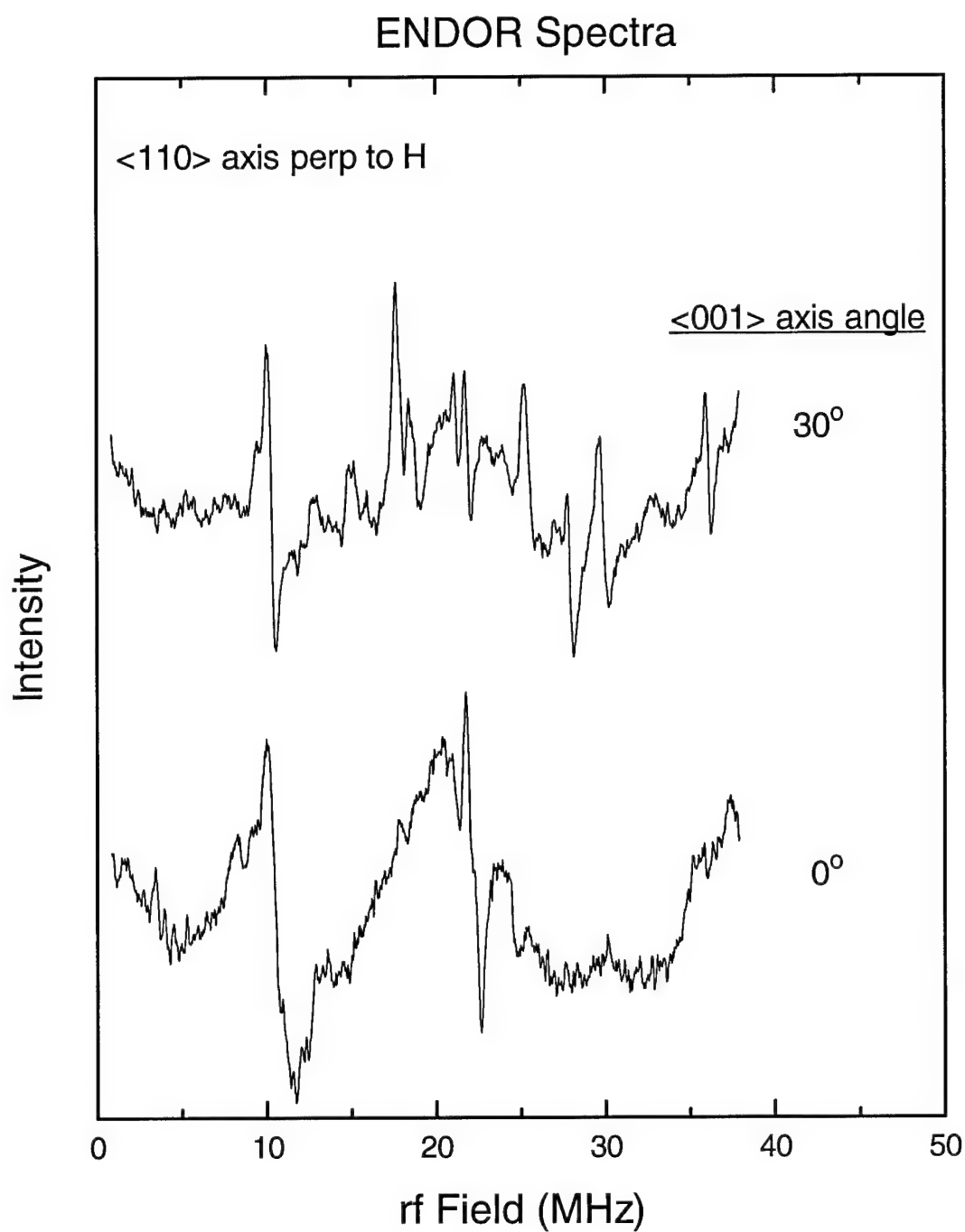Figure 15: Graphical representation of the angular dependence of the features in the EPR spectra shown in figure 7 showing defect symmetry.

Figure 16: ENDOR spectra (saturating peak at 3300 G) at 4 K with magnetic field perpendicular to <110> axis.
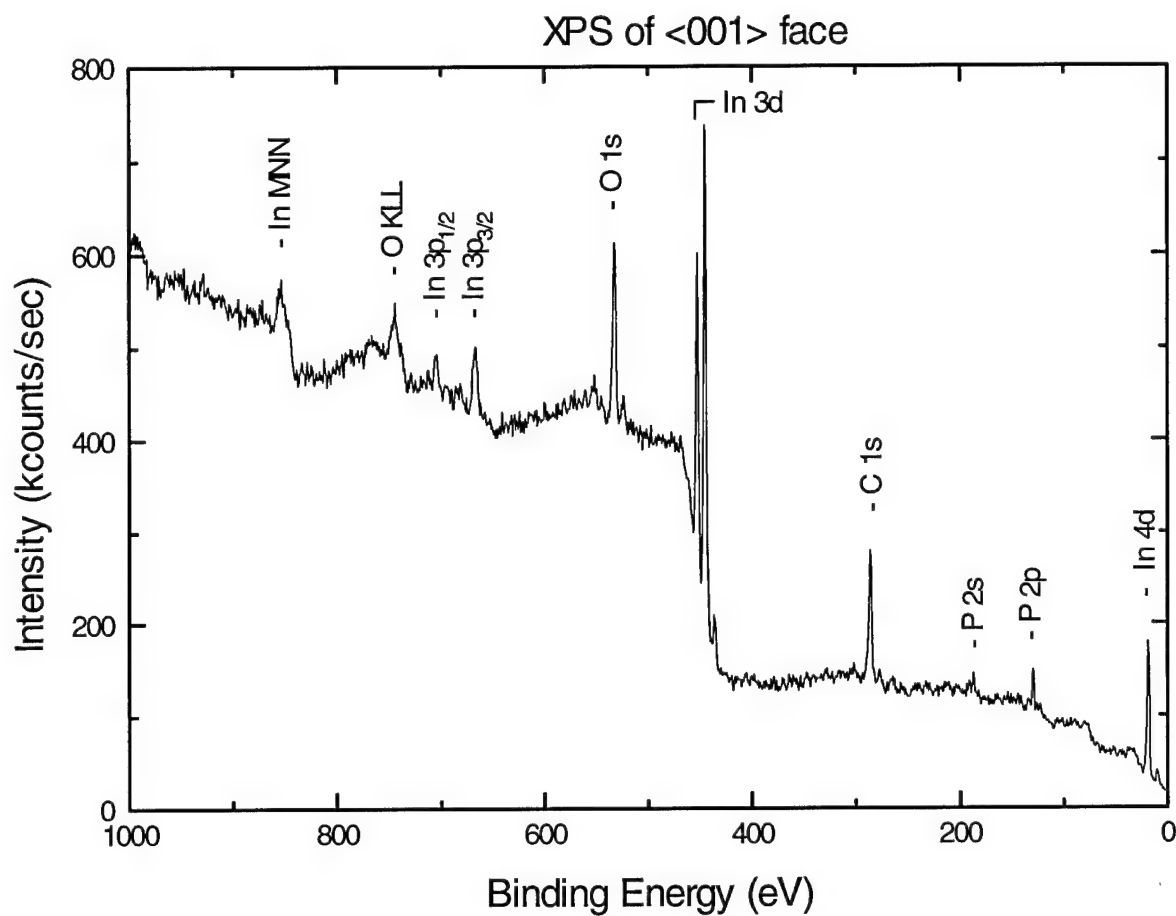
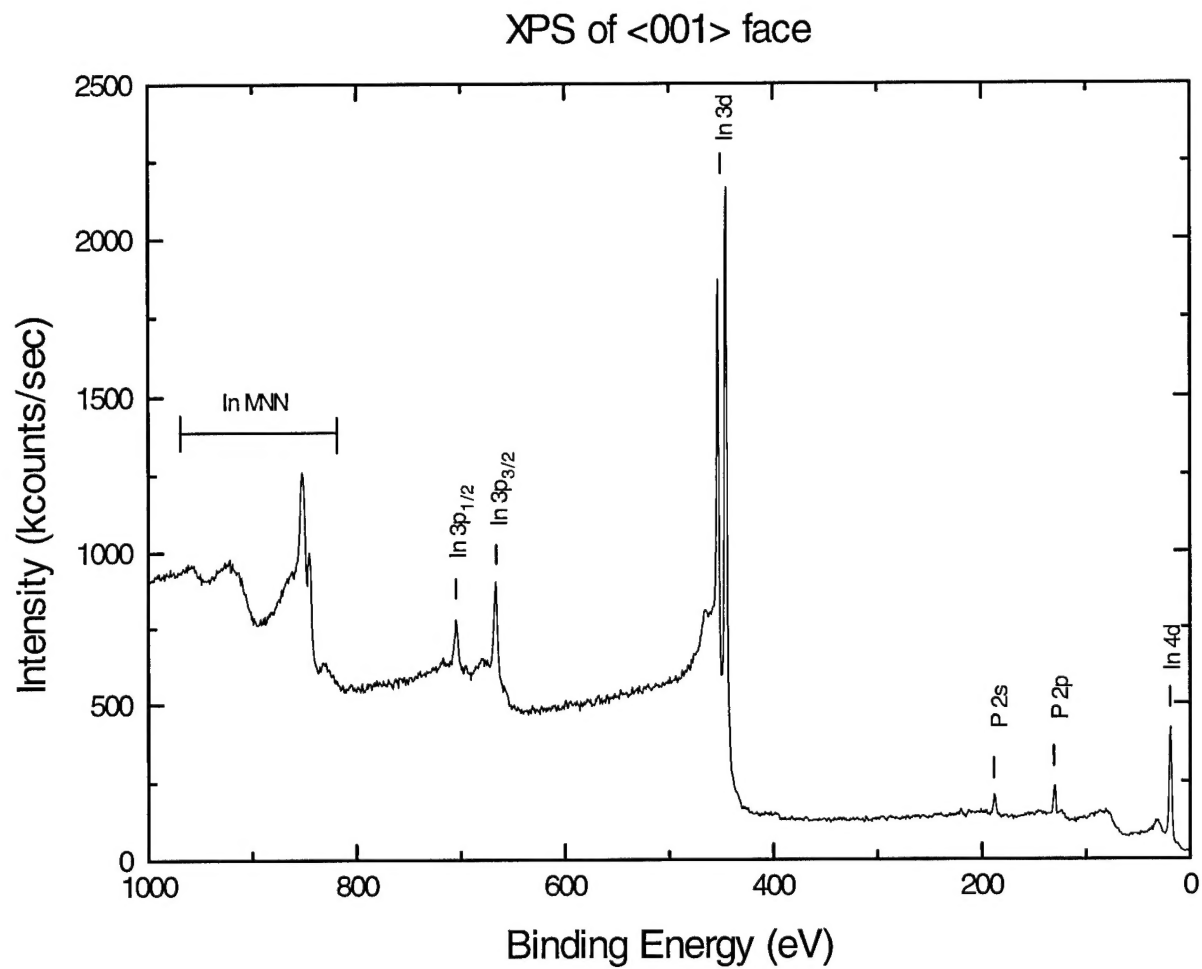Figure 17: XPS spectrum of the [001] face of the Indium Phospide crystal as received.

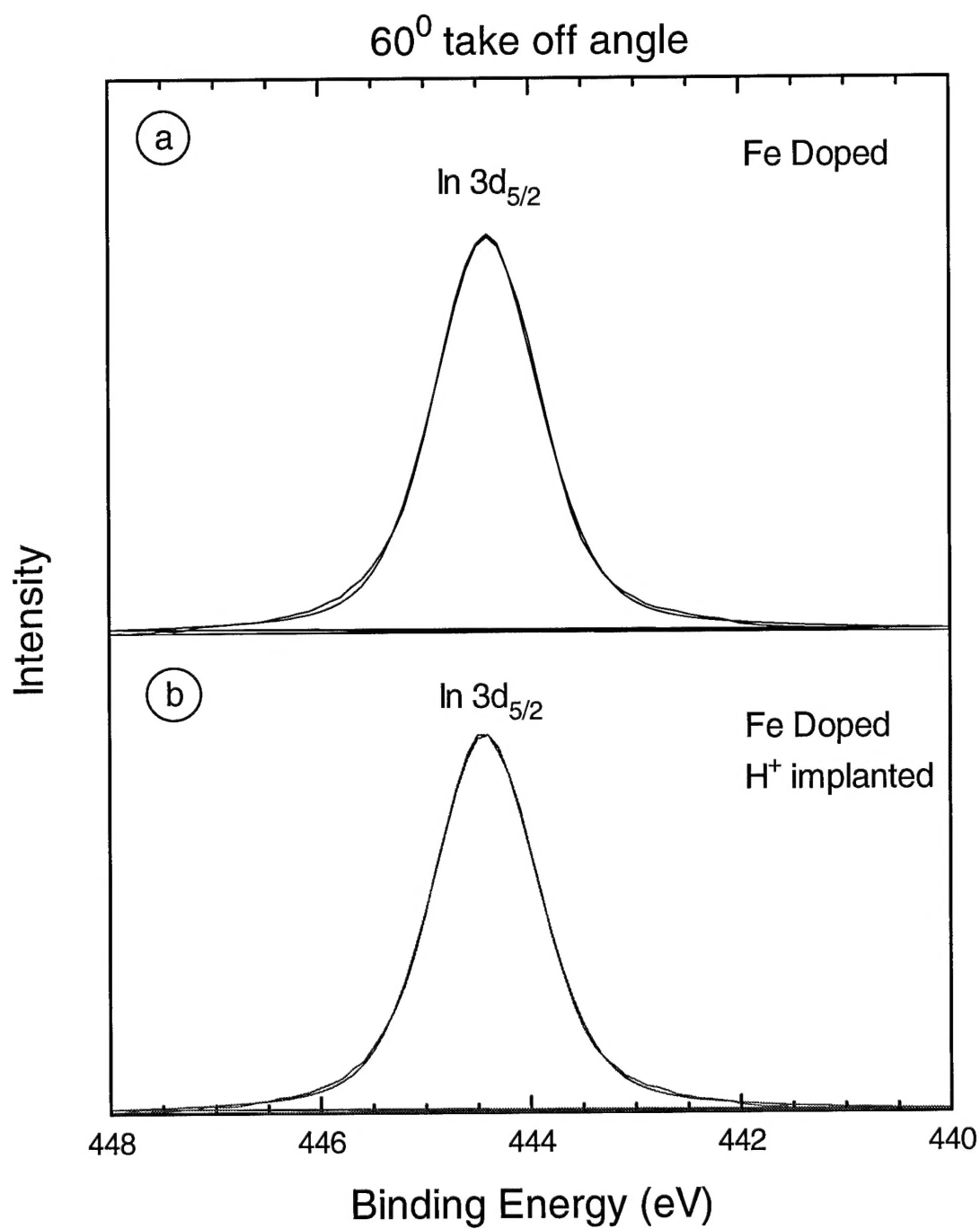Figure 18: XPS spectrum of the [001] face of the Indium Phospide crystal after sputter cleaning.

Figure 19: High resolution, curve fit XPS spectra acquired with the surface normal 30° off the analyser acceptance axis: a) non-polished side of crystal, b) polished, H⁺ implanted side of crystal.
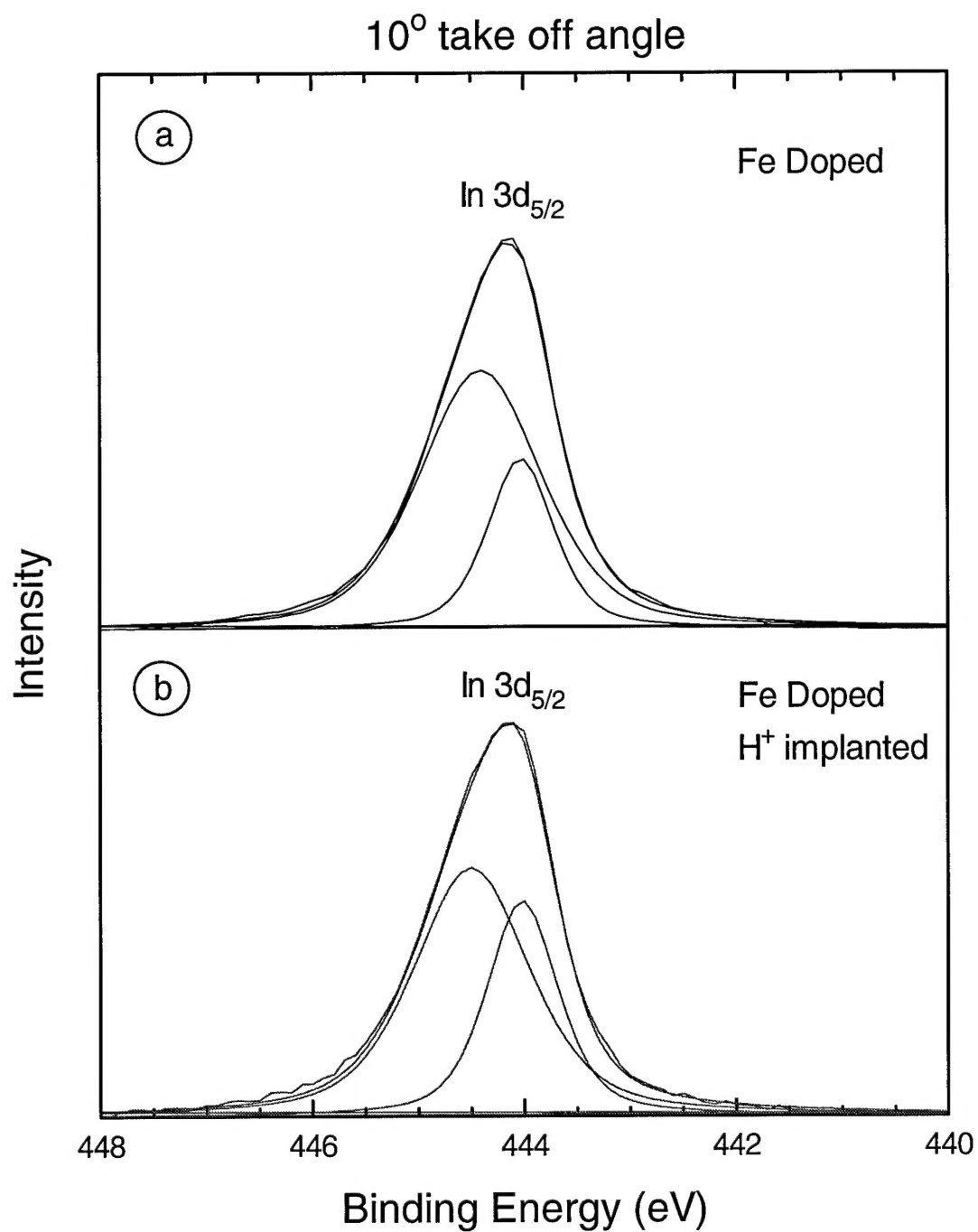
Figure 20: High resolutin, curve fit XPS spectra acquired with the surface normal 80° off the analyser acceptance axis: a) non-polished side of crystal, b) polished, H⁺ implanted side of crystal.
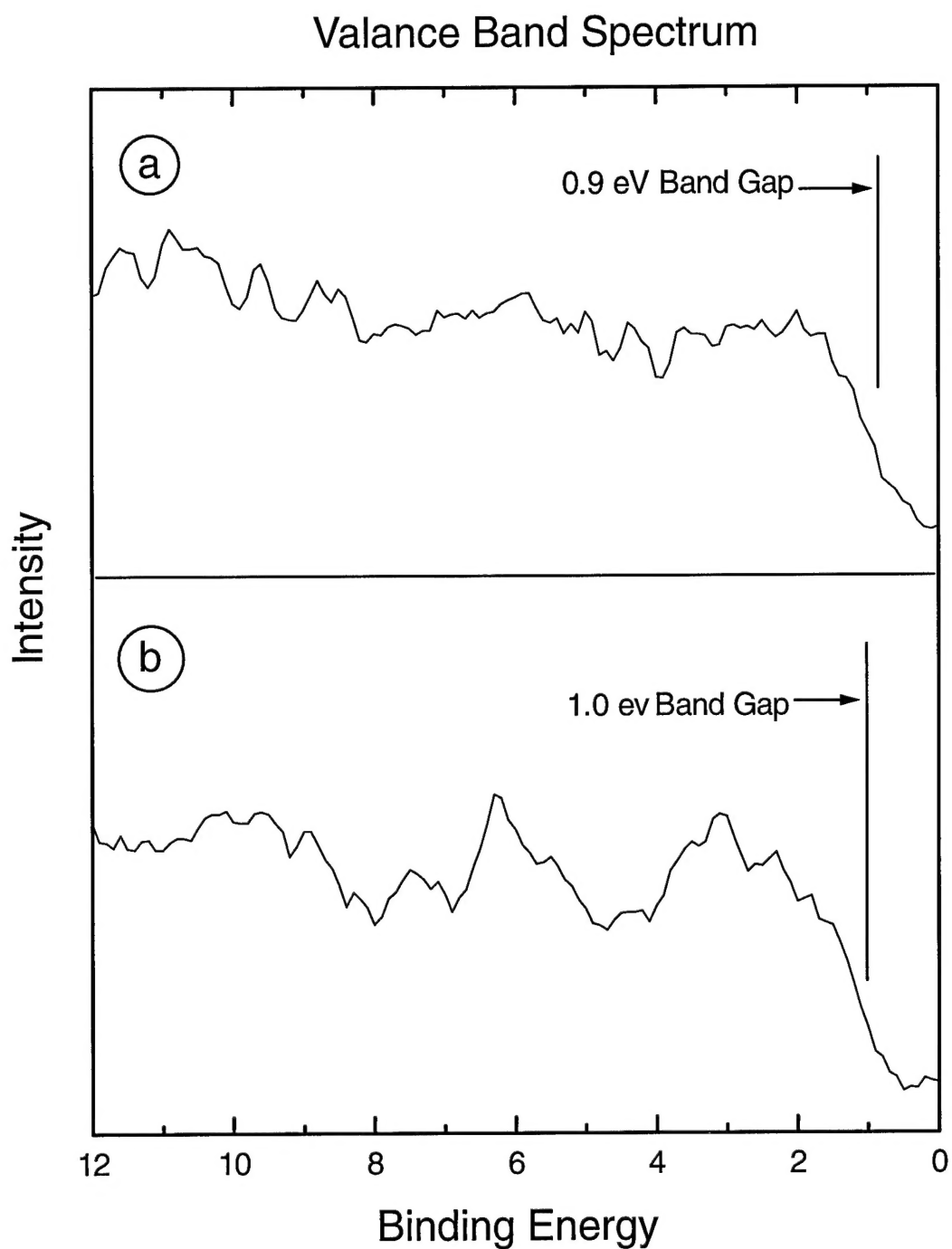
Valance Band Spectrum

Figure 21: High resolutin, XPS of the valence band region of the InP sample: a) non-polished side of crystal, b) polished, H⁺ implanted side of crystal.